Supporting Information

Enhanced Conversion Efficiency in Perovskite Solar Cells by Effectively Utilizing Near Infrared Light

Meidan Que,[a] Wenxiu Que,[a]*, Xingtian Yin,[a] Peng Chen,[a] Yawei Yang,[a] Jiaxing Hu, [a]

Boyan Yu [b] and Yaping Du [b]

Experimental

Synthesis of β-$NaYF_4$: Yb^{3+}, Tm^{3+}/$NaYF_4$ Core-Shell Nanoparticles

β-$NaYF_4$: Yb^{3+},Tm^{3+}/$NaYF_4$ core-shell nanoparticles was synthesized by the technique described in Ref 1. Briefly, firstly, the relevant lanthanide acetates are dissolved in deionized water to obtain the stock solution of 0.2 M lanthanide complexes. Besides, the 1.0 M NaOH solution was prepared by dissolving NaOH in methanol, and a 0.4 M NH_4F solution was prepared by dissolving NH_4F in methanol. Secondly, for the synthesis of $NaYF_4$: Yb^{3+}, Tm^{3+} core, pipette 1 ml of the $Y(CH_3CO_2)_3$ prepared solution, 0.98 ml $Yb(CH_3CO_2)_3$ the prepared solution, 0.02 ml $Tm(CH_3CO_2)_3$ the prepared solution, 6 ml of 1-octadecene and 4 ml of oleic acid into a 50 ml flask. Then the flask was fitted with a thermocouple temperature sensor and the solution was heated to 150 °C for 40 min under stirring, then cooled down gradually until to room temperature. 1 ml NaOH methanol prepared solution and 3.3 ml NH_4F methanol prepared solution were pipetted into the centrifuge tube. Then promptly infuse the mixed solution into the flask. Raise the temperature to 280 °C for 1.5 h. Thirdly, for the synthsis of $NaYF_4$ shell, the steps are the same as those of $NaYF_4$: Yb^{3+}, Tm^{3+} core, except replacing 2.0 ml of the mixture of lanthanide (Y, Yb and Tm) acetates by $Y(CH_3CO_2)_3$ alone and injecting the obtained core particles into the reaction flask before NaOH and NH_4F methanol stock solution was added.

Preparation of TiO_2 Paste

A mixture of TiO_2 (5 mg) and ethyl cellulose (0.1g) was dissolved in 1.7g of terpilenol and 5 ml of ethanol while stirring 20 h, then under ultrasonic treatment for 6h.

Preparation of NYF@TiO_2 Paste

The preparation of the NYF@TiO_2 paste was similar to that of the TiO_2 paste, but the NYF@TiO_2 (5 mg) has different weight ratios (NYF/TiO_2 = 0.125, 0.25, 0.5, 1).

Fabrication of the perovskite solar cells

Prepare the perovskite precursor solution by taking 2.3 g PbI_2 (Weihua-Solar) and 0.8 g CH_3NH_3I (Weihua-Solar) into a 10ml brown bottle with 3.5 ml N,N dimethylformamide (DMF, Alfa-Aesar) and 1.5 ml dimethylsulphoxide (DMSO, Alfa-Aesar) solution at 70℃ under stirring for about 12 h. Then

* Corresponding author:
Tel.: +86-29-83395679; Fax: +86-29-83395679
Email address: wxque@mail.xjtu.edu.cn

filter the resulting solution through the TPFE filter (0.45 mm) to get a bright yellow precursor. Then etch the FTO glass by leveraging the reaction of zinc powder and HCl. Afterward, the patterned substrates were sonicated by in hot solution, including acetone, ethanol, and deionized water, sequentially. The compact TiO_2 layer was spin-coated by the mixed solution of 471 mg of tetrabutyl titanate (ACS, Aladdin) and 109 mg diethanolamine (ACS, Aladdin) in 10 ml ethanol onto the FTO glass at 3000 rpm for 30s, and in the next, by annealing it at 500°C for 60 min. A scaffold layer with a thickness of 150～300 nm was also deposited by using the spin-coating technique. The FTO/compact TiO_2/scaffold layer substrate was immersed in 50 mM aqueous solution of $TiCl_4$ at 60 °C for 60 min. Then, the substrate was rinsed with deionized (DI) water and ethanol, dried by nitrogen blowing, and annealed at 500 °C for 30 min again.

The perovskite precursor solution was infiltrated into the scaffold electrode layer by using the spin-coating process at 1000 rpm for 5s, then 3000 rpm for 30s, the electrode was then heated at 100°C for 30 min. A Chlorobenzene solution containing 72.3 mg/mL of Spiro-OMeTAD, 28.8 μL of tert-butylpyridine, and 35 μL of a solution composed 260 mg of lithium bis(trifluoromethylsyfonyl) imide salt in 1 mL of acetonirtile (99.8%, Aldrich) was cast onto the perovskite coated electrode via a spin-coater at 3000 rpm for 30 s. A 100-nm-thick sliver layer was then evaporated onto the prepared electrode, and the active area of the device was 0.07 cm^2.

Characterization

Scanning electron microscopy (SEM, JSM-6390, JEOL Inc., Japan) was applied to observe the morphology of the films and devices. To observe the microscopic dimension characteristic of the β-$NaYF_4$: (Yb^{3+}, Tm^{3+}) and the β-$NaYF_4$: (Yb^{3+}, Tm^{3+})/$NaYF_4$ Core-Shell nanoparticles, the transmission electron microscope (TEM, Hitachi HT-7700 Inc., Japan) was used. X-ray diffraction (XRD) analysis was used to show the crystalline characteristic of the films from a D/max 2400 X Series X-ray diffractometer (Rigaku, Japan). Photoluminescence emission and excitation measurements were employed utilizing a fluorescence spectrometer (Edinburgh Ltd. FLS920) and a 0.3m double excitation monochromator and 2 emission monochromators (Hamamatsu R928 photomultiplier tube) to record the emission spectra ranging from 200 to 850 nm or ranging from 850 to 1650 nm (Hamamatsu R5509-72 PMT) with a liquid nitrogen-cooled. Temperature-dependent photoluminescence (QM40, PTI) was also measured by a liquid nitrogen-cooled. The UV-Vis absorption spectra of the films were characterized from JASCO V-570 UV/VIS/NIR Spectrometer. The short circuit current density, open circuit voltage, fill factor, and power conversion efficiency of the solar cells were measured in air using a PVIV-201V I-V Station (Newport Oriel). With a Newport 91150V reference cell system, the illumination source was calibrated. For each scan point, the dwell time was altered from 100 ms (scanning rate 100 mV s^{-1}). Unless otherwise stated, performance parameters of all device were obtained with a scanning rate of 100 mV s^{-1}. By keeping the device at the maximum power point for 600 s, the steady state power conversion efficiency of the cells was acquired. Without bias light, the external quantum efficiency (EQE) spectra were recorded in air by using a Qtest Station 1000ADX system (Growntech. Inc). Step for monochromator was 5 nm and chopper frequency180. Dielectric constants of the NYF and perovskite were measured by variable angle spectroscopic ellipsometry (M-2000UI, USA).

Finite-Difference Time-Domain (FDTD) Calculation

Commercially FDTD simulation package, Lumerical, was used to perform the 2-D Full-field electromagnetic wave calculation as qualitative validation for the experimental results. Light direction is parallel to y-axis. Antisymmetric boundary condition is set along the polarization of x-axis and along the propagation of the electromagnetic waves (y-axis), well- matched layers are used. Size of the simulation pitch used is 1000×2200 nm in the x-y plane. The NYF nanoparticle was placed in the middle of the perovskite layer with a diameter of 50 nm. The frequency profile monitor was used to detect the electric fields. All optical material properties used in simulation were measured from experiments under full spectrum.

Conflict of Interest: The authors declare no competing financial interest.

Supplementary Discussion

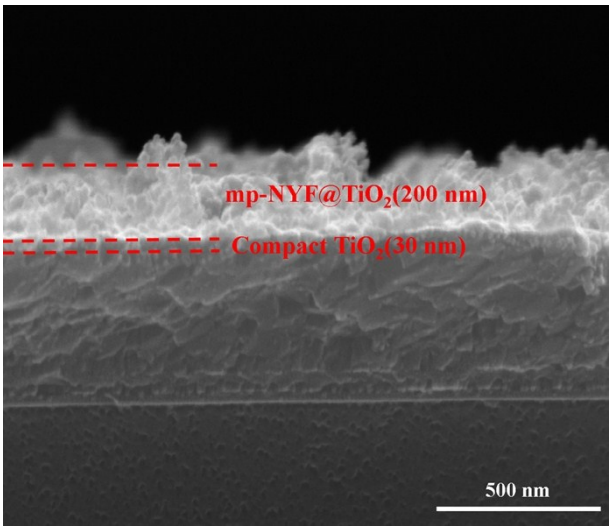

Fig. S1 Cross-sectional SEM images of mp-NYF@TiO_2 scaffold, scale bar, 500 nm.

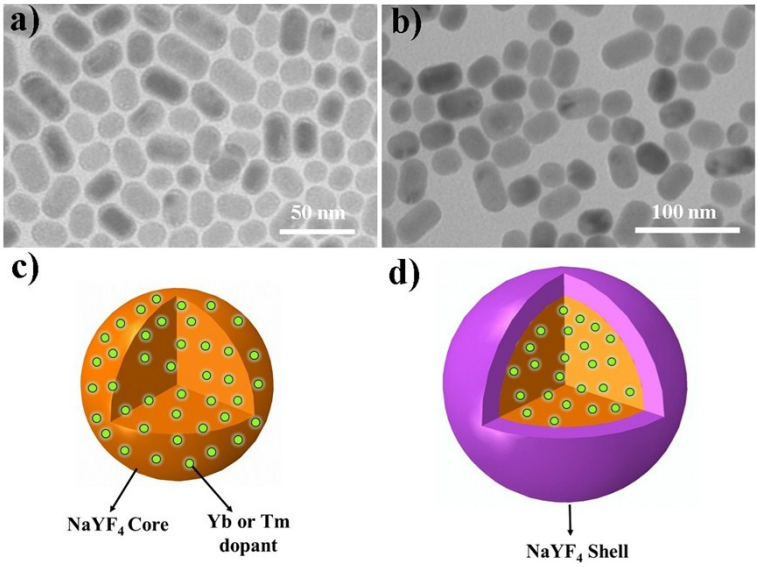

Fig. S2 a) TEM image of $NaYF_4$: Yb^{3+}, Tm^{3+} core nanoparticles; b) TEM image of $NaYF_4$:(Yb^{3+}, Tm^{3+}/$NaYF_4$ core-shell nanoparticles; c) and d) the corresponding schematic diagram of the core/shell

nanoparticles.

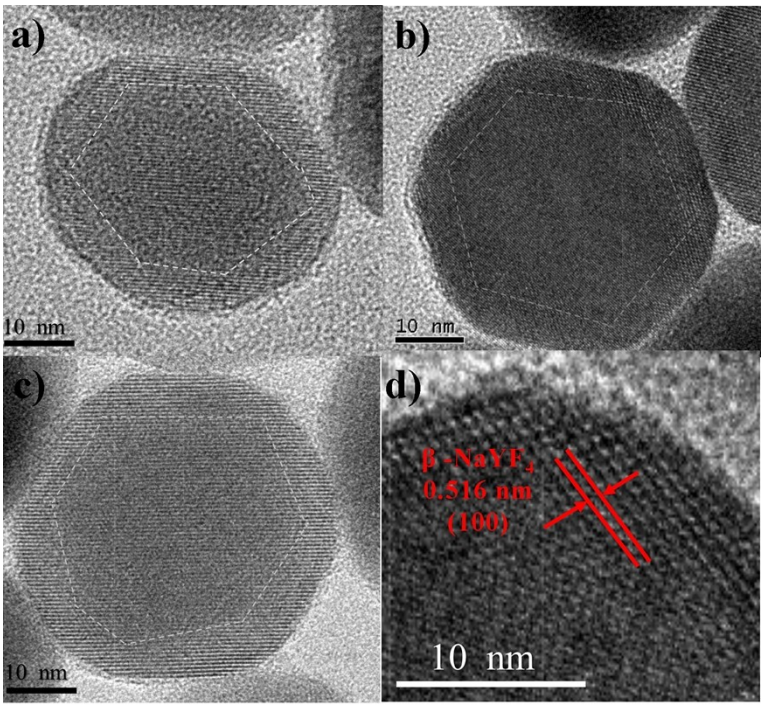

Fig. S3 Representative TEM images of the core–shell structure of β-$NaYF_4$: Yb^{3+}, Tm^{3+}/$NaYF_4$ nanoparticles.

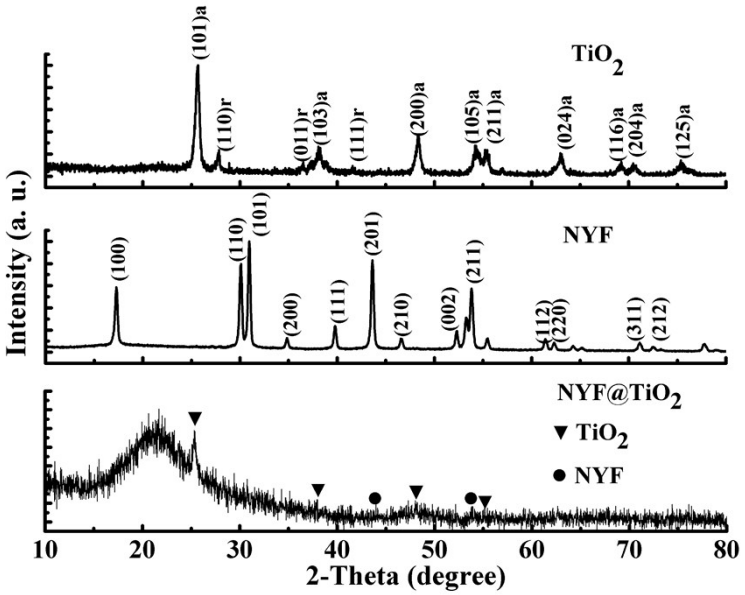

Fig. S4 XRD patterns of TiO_2, NYF, and the paste of NYF@TiO_2 sintered at 450°C for 1h in air.

The XRD patterns of TiO_2, NYF and NYF@TiO_2 powders are shown in Fig. S4. It is noticed that the diffraction peaks of TiO_2 can be exactly assigned to the anatase and rutile phases, which can be indexed as (101), (103), (200), (105), (211), (024), (116), (204) and (115) planes of anatase TiO_2 (JCPDS 21-1272), respectively, besides (110), (011) and (111) planes of rutile TiO_2 (JCPDS 21-1276). After sintering the NYF@TiO_2 paste, several new peaks corresponding to (111) and (211) planes of

NYF_4 (JCPDS 16-0334) appear, indicating the presence of NYF.

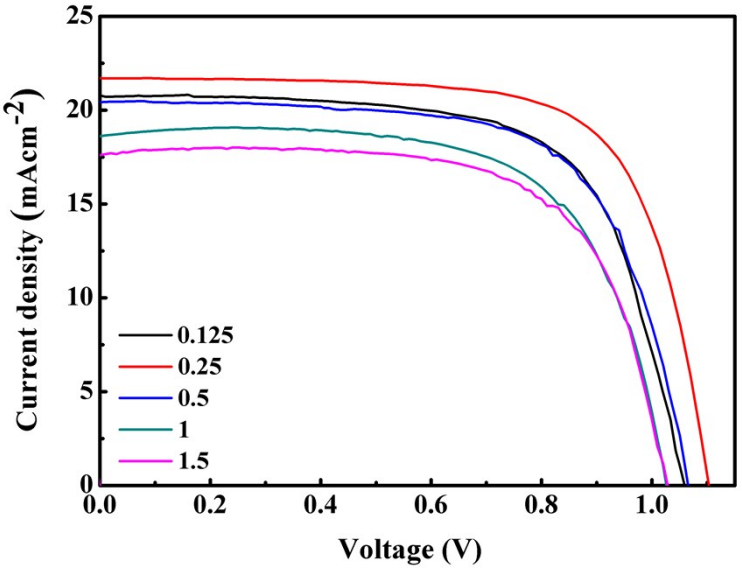

Fig. S5 J-V curves of the devices with different weigh ratios of NYF/TiO_2.

Table S1 The optimized short-circuit current density (J_{sc}), open-circuit voltage (V_{oc}), fill factor (FF) and power conversion efficiency (PCE) of the perovskite solar cells with different weigh ratios of NYF/TiO_2.

NYF/TiO_2 ratio	V_{oc} (V)	J_{sc} ($mAcm^{-2}$)	FF (%)	PCE (%)
0.125	1.05	20.8	67.1	14.7
0.25	1.08	21.4	68.7	16.0
0.5	1.06	20.5	66.9	14.6
1.0	1.02	18.6	66.8	12.7
1.5	1.03	17.6	67.6	12.2

Fig. S5 shows the photocurrent-voltage curves of the devices with different weigh ratios of $NYF@TiO_2$, and the corresponding photovoltaic parameters are listed in Table S1, where the average short-circuit J_{sc}, V_{oc}, FF and PCE are estimated. It can be seen from Fig. S5 and Table S1 that J_{sc} increases with an increase of the $NYF@TiO_2$ weight ratio and then decreases with further increase of the $NYF@TiO_2$ weight ratio, but there are no obvious changes for V_{oc} and FF. This implies that J_{sc} is related to the amount of the NYF NPs.

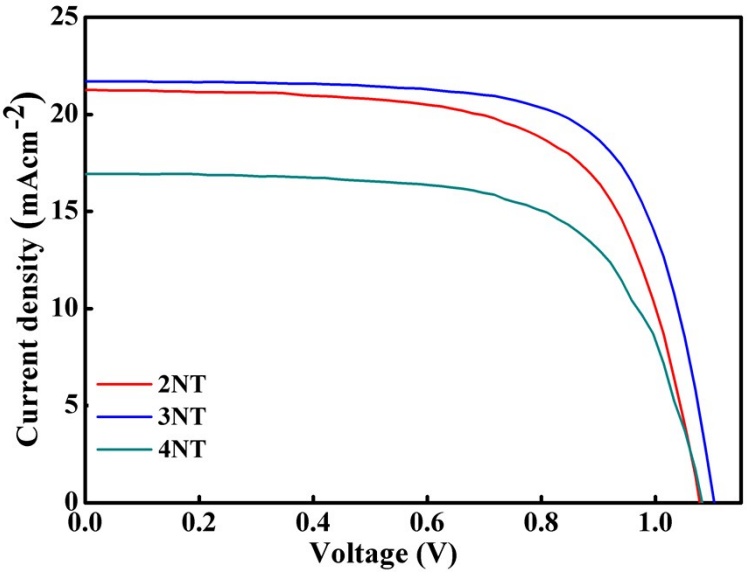

Fig. S6 J-V curves of the devices with different thicknesses of NYF@TiO_2.

Table S2 J_{sc}, V_{oc}, FF and PCE of the perovskite solar cells with different thicknesses of NYF@TiO_2 scaffold.

sample	V_{oc} (V)	J_{sc} ($mAcm^{-2}$)	FF (%)	PCE (%)
2NT	1.08	21.2	66.5	15.2
3NT	1.10	21.7	70.6	16.9
4NT	1.01	19.6	68.4	13.6

"2NT device", "3NT device" and "4NT device" are composed of two, three and four layers of the NYF@TiO_2 nanocomposites, respectively. These nanocomposites were sintered at 450 °C for 1 h in air, and then these as-obtained porous networks were immersed into 50 mM $TiCl_4$ aqueous solution for 1h. Finally, the as-prepared scaffolds were calcined at 450 °C for 0.5 h in air again. In order to optimize the structure of the NYF@TiO_2 modified ETL, the corresponding solar cells were assembled and tested as shown in Fig. S6, the optimized photovoltaic parameters are listed in Table S2. It can be seen that with increasing the layer number of the NYF@TiO_2 nancomposite from two layers to three layers, the V_{oc} increases from 1.08 to 1.10 V, the J_{sc} and FF also increase from 21.2 to 21.7 $mAcm^{-2}$ and from 66.5 to 70.6%, respectively. It is probably related to that the uniformity of the perovskite coating upon the scaffold is improved. **Actually, the pin-holes and "shunting paths" can be reduced as the scaffold thickness increases, thus increasing the light-harvesting efficiency.** However, as the layer number of the NYF@TiO_2 nanocomposite further increases to four layers, the PCE and J_{sc} decreases to 13.6% and 19.6 $mAcm^{-2}$, respectively. We think that the decrease of the J_{sc} and FF should be ascribed to the competition between the electron recombination and the charge collection.[2]

Table S3 The average V_{oc}, J_{sc}, FF and PCE of the TiO_2 and NYF@TiO_2-based device.

sample	V_{oc} (V)	J_{sc} (mAcm^{-2})	FF (%)	PCE (%)
TiO_2	1.08	20.1	65.0	13.8
NYF@TiO_2	1.09	20.8	66.4	15.1

In order to better understand that J_{sc} is related to the NYF@TiO_2 nanocomposite, the MSCs employing only the NYF NPs was fabricated and termed as "NYF device", which has the same thickness to the "3NT device". The measured performances of the NYF device are not as good as TiO_2 devices. Furthermore, "3NT w/o $TiCl_4$ device", which has the same components as the "3NT device" but without $TiCl_4$ aqueous solution treatment, was also fabricated. Results show that the "3NT w/o $TiCl_4$ device" has inferior J_{sc} of 12.1 mA cm^{-2} and FF of 36.4% as compared with the "3NT device".

Table S4 The optimized Voc, Jsc, EQE, FF, transient PCE, steady state PCE of the TiO_2 and NYF@TiO_2-based device

sample	V_{oc} (V)	J_{sc} (mAcm^{-2})		FF (%)	PCE (%)	
		J-V	EQE		J-V	Steady-state
TiO_2	1.08	19.8	16.2	65.9	14.1	13.9
NYF@TiO_2	1.10	21.7	17.1	70.6	16.9	16.8

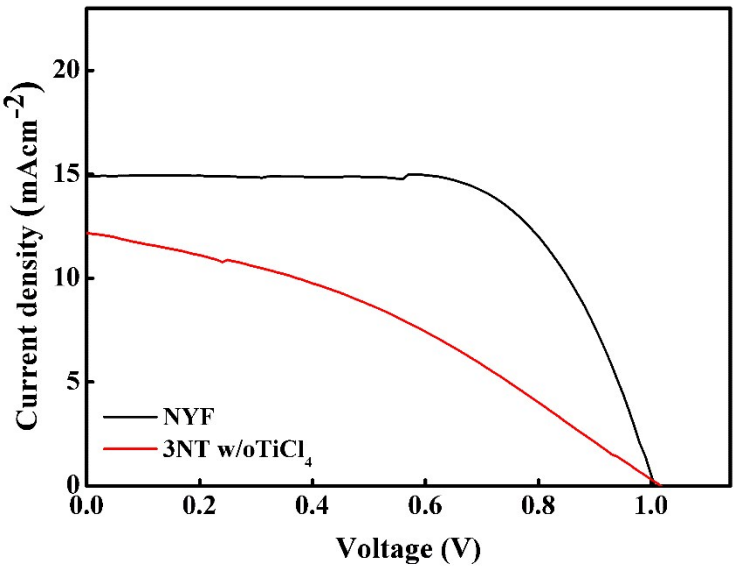

Fig. S7 J-V curves of the NYF-based and NYF@TiO_2-based devices.

Table S5 J_{sc}, V_{oc}, FF and PCE of NYF device and 3NT w/o $TiCl_4$ device.

sample	V_{oc} (V)	J_{sc} ($mAcm^{-2}$)	FF (%)	PCE (%)
NYF	1.00	14.9	67.3	10.1
3NT w/o$TiCl_4$	1.01	12.1	36.4	4.5

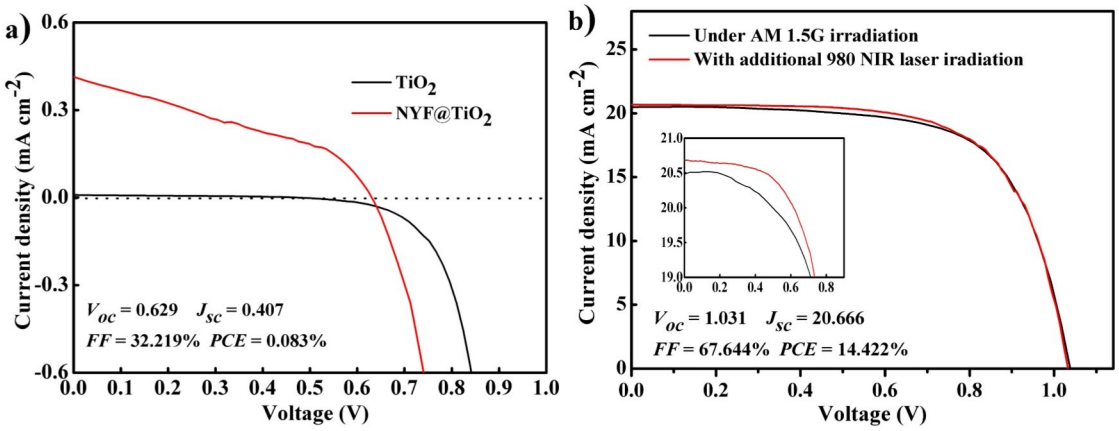

Fig. S8 a) The J-V curves of NYF@TiO_2-based device and TiO_2-based device under 980 nm NIR laser light; b) the typical efficiencies of NYF@TiO_2-based device under an AM1.5G standard sunlight and an additional 980 nm NIR laser.

References

1. F. Wang, R. R. Deng, X. G. Liu, *Nat. Photonics.*, 2014, 7, 1634-1644.
2. J. M. Ball, M. M. Lee, A. Hey, H. J. Snaith, *Energy Environ. Sci.*, 2013, 6, 1739-1743.